Molecular Biology of the Cell
Vol. 18, 1507–1518, April 2007

The Myosin IXb Motor Activity Targets the Myosin IXb RhoGAP Domain as Cargo to Sites of Actin Polymerization[D] [V]

Frank van den Boom,* Heiko Düssmann,*† Katharina Uhlenbrock,* Marouan Abouhamed, and Martin Bähler

Institute for General Zoology and Genetics, Westfalian Wilhelms-University, 48149 Münster, Germany

Submitted September 5, 2006; Revised December 26, 2006; Accepted February 5, 2007
Monitoring Editor: Paul Forscher

Myosin IXb (Myo9b) is a single-headed processive myosin that exhibits Rho GTPase-activating protein (RhoGAP) activity in its tail region. Using live cell imaging, we determined that Myo9b is recruited to extending lamellipodia, ruffles, and filopodia, the regions of active actin polymerization. A functional motor domain was both necessary and sufficient for targeting Myo9b to these regions. The head domains of class IX myosins comprise a large insertion in loop2. Deletion of the large Myo9b head loop 2 insertion abrogated the enrichment in extending lamellipodia and ruffles, but enhanced significantly the enrichment at the tips of filopodia and retraction fibers. The enrichment in the tips of filopodia and retraction fibers depended on four lysine residues C-terminal to the loop 2 insertion and the tail region. Fluorescence recovery after photobleaching and photoactivation experiments in lamellipodia revealed that the dynamics of Myo9b was comparable to that of actin. The exchange rates depended on the Myo9b motor region and motor activity, and they were also dependent on the turnover of F-actin. These results demonstrate that Myo9b functions as a motorized RhoGAP molecule in regions of actin polymerization and identify Myo9b head sequences important for in vivo motor properties.

INTRODUCTION

In cells the actin cytoskeleton and signal transduction are closely interlinked. Many different signaling pathways impinge on actin-binding proteins that regulate actin organization and dynamics. Vice versa the actin cytoskeleton regulates the spatial distribution and activity of various signaling molecules. We have proposed previously that class IX myosins could represent actin-based motorized signaling molecules (Bähler, 2000). Although the mammalian class IX myosin Myo9b (formerly also called myr 5) is a single-headed myosin, in vitro actin-gliding assays revealed that it takes many successive steps along actin filaments without dissociating, implying that it is a processive motor molecule (Inoue *et al.*, 2002; Post *et al.*, 2002; Nishikawa *et al.*, 2006). However, kinetic analysis of Myo9b demonstrated that it spends during its ATPase cycle considerable time in the ATP-bound state, a state in which other myosins typically are not associated with actin filaments (Nalavadi *et al.*, 2005; Kambara and Ikebe, 2006). A long insertion in loop 2 (50/20-kDa junction) of the Myo9b head domain that is specific to class IX myosins, has been proposed to act as an actin tether keeping the single headed Myo9b attached to the actin filament in the ATP-bound state. Indeed, Myo9b exhibits a relatively high-affinity for F-actin in the ATP-bound state (Nalavadi *et al.*, 2005; Kambara and Ikebe, 2006). In addition to the question of Myo9b processivity, a further unresolved issue concerns the directionality of Myo9b movement along the polar actin filaments. In vitro, Myo9b affinity adsorbed from tissue extracts showed movement toward the plus-end of actin filaments (O'Connell and Mooseker, 2003) whereas truncated recombinant Myo9b moved toward the minus-end (Inoue *et al.*, 2002). Currently, it is not known whether and if so, how Myo9b motor activities could be regulated.

In addition to a characteristic myosin head domain myosins contain different tail domains that either self-assemble, bind cargo and/or regulate motor activity (Krendel and Mooseker, 2005). The tail domains of class IX myosins encompass a RhoGTPase-activating protein (RhoGAP) domain (Reinhard *et al.*, 1995). GAPs catalyze the inactivation of G-proteins by accelerating GTP-hydrolysis and thereby switching them from the GTP-bound active conformation to the GDP-bound inactive conformation (Scheffzek *et al.*, 1998). The RhoGAP activity of Myo9b critically depends on a conserved arginine residue that stabilizes the transition state during GTP hydrolysis (Ahmadian *et al.*, 1997; Müller *et al.*, 1997; Graf *et al.*, 2000). Both in vitro and in vivo, the Myo9b GAP domain shows a preferential specificity for Rho A, B, and C of the tested Rho-subfamily members of monomeric G-proteins (Müller *et al.*, 1997). Many Rho-subfamily GAPs have been characterized in eukaryotes (Moon and Zheng, 2003). However, very little is known about their in vivo functions that might be controlled by dynamic interactions with additional proteins regulating their subcellular localizations and/or RhoGAP activities (Bernards and Settleman, 2004). Myo9b has been localized to dynamic re-

This article was published online ahead of print in *MBC in Press* (http://www.molbiolcell.org/cgi/doi/10.1091/mbc.E06–08–0771) on February 21, 2007.

[D] [V] The online version of this article contains supplemental material at *MBC Online* (http://www.molbiolcell.org).

* These authors contributed equally to this work.

† Present address: Department of Physiology and Medical Physics, Royal College of Surgeons in Ireland, York House, York Street, Dublin 2, Ireland.

Address correspondence to: Martin Bähler (baehler@uni-muenster.de).

gions of the cell periphery, the Golgi-area, and the cytosol (Müller *et al.*, 1997). In cells infected with the pathogenic bacterium *Shigella flexneri*, Myo9b was found to colocalize with RhoC, but not RhoA, in the tips of actin-rich circular membrane ruffles induced by the bacteria (Graf *et al.*, 2000). How the subcellular localization of Myo9b with its RhoGAP activity is determined and regulated is not known. The local accumulation of a RhoGAP will either enhance the cycling rate of Rho between the inactive and active conformations or reduce the concentration of active Rho. The organization of the actin cytoskeleton that is controlled by Rho-family members is likely to influence subcellular targeting of the motor protein Myo9b. This hypothesis is especially intriguing as Rho activity is known to control the organization of the actin cytoskeleton through modulation of actin-binding proteins and via cross-talk with other Rho-family members (Ridley and Hall, 1992; Sander *et al.*, 1999; Tsuji *et al.*, 2002; Nimnual *et al.*, 2003; Wang *et al.*, 2003). Therefore, the motor and RhoGAP domains of Myo9b may mutually influence each other.

Here we determined the dynamic subcellular localization of Myo9b in melanoma cells plated on laminin and analyzed the respective contributions of the different regions and activities. We also studied the Myo9b motor properties in extending lamellipodia in vivo by fluorescence recovery after photobleaching (FRAP) and photoactivation experiments. To avoid severe morphological changes of cells expressing the Myo9b constructs, we introduced a point mutation in the RhoGAP domain (R1695M) that virtually abolishes RhoGAP activity (Müller *et al.*, 1997).

MATERIALS AND METHODS

Cell Culture and Cell Transfections

B16/F1 mouse melanoma cells (American Type Culture Collection, Manassas, VA) were cultured in high glucose DMEM (Invitrogen, Karlsruhe, Germany) supplemented with 10% fetal calf serum (FCS; Biochrom, Berlin, Germany), 2 mM L-glutamine (Invitrogen, Karlsruhe, Germany), 50 U/ml penicillin (Invitrogen), and 0.05 mg/ml streptomycin (Invitrogen) at 37°C in a humidified atmosphere with 5% CO_2.

For transfection B16/F1 cells were cultured on Ø 40-mm dishes and transfected by using SuperFect reagent (QIAGEN, Hilden, Germany). Transfected cells were replated after >16 h on sterile, laminin-coated coverslips and incubated for an additional 4 h before analysis. Coverslips were coated for 1 h with 25 μg/ml laminin (Sigma-Aldrich, Munich, Germany) in coating buffer (150 mM NaCl, 50 mM Tris, pH 7.5) and rinsed with PBS (150 mM NaCl, 3 mM Na_2HPO_4, 1.5 mM KH_2PO_4, pH 7.4) immediately before plating of cells.

For the photoactivation experiments cells were plated on mouse laminin (Sigma)-coated 30 mm glass-bottom dishes (MatTek, Ashland, MA) and transiently transfected overnight with different PAGFP-constructs using Superfect transfection reagent (QIAGEN) according to the manufacturer's protocol. To localize transfected cells, they were cotransfected with mRFP-actin in a ratio of 7:3 (PAGFP-X:mRFP-actin) to obtain a total DNA amount of 1 μg. Cells were analyzed 15–24 h after transfection.

Construction of Plasmids

The different expression plasmids encoding enhanced green fluorescent protein (EGFP) and PAGFP rat Myo9b fusion proteins were constructed according to standard molecular biology protocols. A detailed description of their construction is given in the Supplementary Materials and Methods. The plasmid encoding mRFP-actin was a kind gift from Klemens Rottner (Braunschweig, Germany) and Roger Tsien (San Diego, CA).

Labeling of Cells, Epifluorescence Microscopy, and Quantitation of Cell Extensions

B16/F1 cells growing on laminin-coated coverslips were fixed in 4% paraformaldehyde (PFA; Merck, Darmstadt, Germany) for 30 min. Excess aldehyde groups were quenched with 0.1 M glycine (Roth, Karlsruhe, Germany) for 10 min, and then cells were permeabilized in 0.05% saponin (Sigma) for 20 min. Unspecific binding sites were blocked with 5% normal goat serum (NGS; Dianova, Hamburg, Germany). All reagents were buffered with PBS. F-actin was labeled with Alexa 594- or Alexa 350-conjugated phalloidin (Molecular Probes, Eugene, OR) diluted in NGS/PBS. Finally, the coverslips were inverted and mounted in mowiol on microscope slides. The cells were analyzed with an Axiophot fluorescence microscope (Carl Zeiss, Göttingen, Germany) by using Plan-Neofluar 63× or 100× oil immersion objectives (NA 1.25 and 1.3, respectively). Images were acquired with an ORCA-285digital camera (Hamamatsu Photonics, Herrsching, Germany) controlled by Wasabi software (version 1.4; Hamamatsu). Images were processed in Adobe Photoshop 7.0 (San Diego, CA).

Cell extensions were defined as thin (<1 μm) phalloidin-stained, nonbranched protrusions that extended at least 1 μm from the cell margin. The number of cell extensions was determined per micron of cell perimeter. Extensions that showed a clearly increased GFP (green fluorescent protein) fluorescence at their tips were counted separately. Significance was determined according to a one-way ANOVA test. As a multiple comparison post test the Tukey test was applied (Prism 3.0, Graph Pad Software, San Diego, CA). Data with a p-value <0.05 were considered to be significantly different.

Total Internal Reflection Fluorescence Microscopy

B16/F1 cells expressing GFP-Myo9b constructs were grown on laminin-coated coverslips for 24 h and fixed, quenched, and permeabilized as described above. F-actin was stained with Alexa594-Phalloidin (Molecular Probes). After staining, cells were kept in PBS and mounted in an open homemade cell chamber and covered with PBS. Cells were imaged using a TILL-total internal reflection fluorescence (TIRF) system (TILL-Photonics, Gräfelfing, Germany) equipped with a 60× PlanApo TIRFM (NA 1.45) objective (Olympus Europe, Hamburg, Germany) and an IMAGO S-VGA camera (TILL photonics) or a VisiTIRF system (Visitron, Pucheim, Germany) using a Zeiss 100× Plan Fluar objective (NA 1.45) and a Cascade II back-illuminated EMCCD camera (Roper Scientific, Ottobrunn, Germany). Illumination at 488 or 568 nm was achieved by either a 75-mW Ar (Spectra-Physics, Bedford, MA) and a 20-mW Kr laser (Melles Griot, Rochester, NY) or a 20-mW Ar/Kr laser (Melles Griot).

Live Cell Imaging and Fluorescence Recovery after Photobleaching

For live cell imaging and fluorescence recovery after photobleaching (FRAP) experiments, B16/F1 cells growing on laminin-coated coverslips were transferred into a homemade cell chamber and covered with HEPES-buffered Ham's F12 medium (Sigma) containing 10% FCS. For the duration of the experiments, the cells were maintained at 37°C on a heating stage. Live cell imaging and FRAP experiments were performed with a laser scanning microscope (LSM 510, software version 2.8; Zeiss) using the 458-, 477-, and 488-nm emission bands of the Ar laser with 6-Å tube current and a 63× NA 1.4 Plan-Apochromat oil immersion objective. For imaging of the cells, the laser power was attenuated to 1%, and the pinhole was adjusted to 1-μm vertical resolution and 0.2-μm lateral resolution scanned in the bidirectional mode. FRAP experiments were performed in the lamellipodia of cells moving for 10–30 min before and after FRAP experiments. In FRAP experiments, bleaching was performed after the tenth image within a 2-μm-wide rectangle (vertical direction) using five iterations of the 458-, 477-, and 488-nm lines while the acusto-optical tunable filter (AOTF) was set to 100% transmission. For the determination of the recovery kinetics the acquired image stacks consisting of at least 150 images were processed in Metamorph 6.1 (Universal Imaging, Visitron, Germany). The average intensity in the bleached region was calculated after background subtraction and corrected for bleaching due to rapid image acquisition.

Average recovery curves for each construct, normalized to the bleached fraction, were fitted to biexponential functions of the following form:

$$f(t) = F(t_\infty) - F1e^{-(t/t1)} - F2e^{-(t/t2)} \quad (1)$$

using Microcal Origin 7.5 software. $F(t_\infty)$ is the mobile fraction of the fluorophores, F_{fast} (F1) is the amplitude of a fast, and F_{slow} (F2) the amplitude of a slowly recovering population of molecules. The immobile fraction is simply calculated as $F_{imm} = 1 - F(t_\infty)$. Recovery kinetics were determined with t1 and t2 for the fast and slow fraction, respectively, which can be recalculated as rates, e.g., $k1 = 1/t1$.

Photoactivation Experiments

Photoactivation experiments were performed with an Olympus FV-1000 (Olympus Europe) dual-headed laser scanning microscope equipped with an incubation chamber to ensure a controlled atmosphere (37°C, 5% CO_2, 30% relative humidity; for PAGFP) or a Zeiss LSM 510 Meta laser scanning microscope (other constructs) equipped with a heating stage and an objective heater adjusted to 37°C.

Cells were covered with MEM (Sigma) supplemented with either 2.2 g/l $NaHCO_3$, pH 7.4, for experiments under controlled CO_2 conditions or 30 mM HEPES, pH 7.4, respectively. Cells potentially expressing PAGFP constructs were localized by the fluorescence of the cotransfected mRFP-actin. Experiments were performed by trying to activate a region of interest (ROI) at the lamellipodium of a mRFP-actin–positive cell.

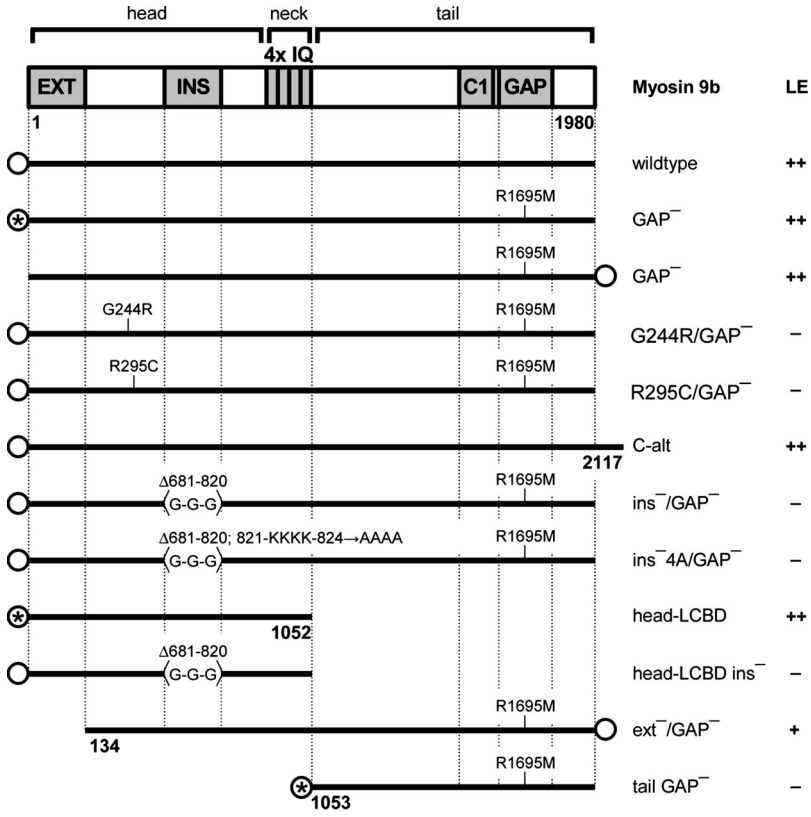

Figure 1. Schematic representation of rat Myo9b EGFP-constructs and summary of their localizations. Mutated residues, deletions, and truncations are indicated. Note individual regions are not drawn to scale. Ext, extension; ins, loop 2 insertion; IQ, IQ-motif; C1, Zn^{2+}-binding domain; GAP, RhoGAP domain, O, EGFP (* constructs additionally existing as photoactivatable variants). Localization in regions of actin polymerization (LE, leading edge) is indicated as follows: ++, enriched; +, present; and −, not present. Numbers indicate the corresponding amino acids.

Using the Zeiss LSM 510 Meta, lamellipodia were imaged with a Plan-Apochromat 100× objective (NA 1.4). To image the cells, the 488-nm laser line of an Argon Laser (6.5-Å tube current) and the 543-nm laser line of a HeNe laser were used in the single scanning mode, and the pinhole was set to the maximum diameter.

To follow the fast kinetics of PAGFP, an Olympus FV-1000 microscope equipped with a PlanApo 60× objective (NA 1.1) was used, and photoactivation was performed with the SIM scanner during image acquisition. The laser and pinhole adjustments were the same as in the experiments with the Zeiss LSM 510. After imaging 10 frames, a rectangular region at the leading edge perpendicular to the main direction of lamellipodial migration was photoactivated by a single iteration using a 405-nm laser diode with full laser power. The photoactivated region had a height of 2 μm, and its width was variable, depending on the form of the lamellipodium. The cells were imaged for 200–300 images after photoactivation, i.e., 15–50 s.

Images of the GFP-channel were processed using ImageJ 1.33. After subtracting the average background intensity from a nonactivated region inside the cell, the average fluorescence intensity was extracted from the region of interest. The first time point after photoactivation was set to t = 0 and the time dependent decay of the PAGFP-fluorescence intensity was plotted over time. Normalized data were fitted to biexponential decays using the following equation (Sigma Plot 7.0, SPSS):

$$f(t) = F_{imm} + F1e^{-t \bullet k1} + F2e^{-t \bullet k2} \quad (2)$$

with the following constraints: $k1 > 0$; $k2 > 0$; $F_{imm} > 0$.

The rates of exchange k1 and k2 were recalculated to the time constants $t1,2 = 1/k1,2$.

All values given for PAGFP and FRAP experiments are mean values ± SEM. One-way ANOVAs and least significant differences were calculated with SPSS 11.0 (Lead Technologies, Charlotte, NC). $p < 0.05$ was considered to indicate significant differences.

RESULTS

Myo9b Localizes to Regions of Newly Polymerizing F-Actin

To determine the dynamic subcellular distribution of Myo9b in living cells, we expressed several Myo9b constructs fused to EGFP in mouse melanoma B16/F1 cells (for overview of constructs see Figure 1 and for their expression see Supplementary Figure S1). The RhoGAP activity of overexpressed Myo9b led to considerable morphological changes. Because EGFP-Myo9b with a point mutation (R1695M; GAP⁻) that abrogates its RhoGAP activity (Müller *et al.*, 1997) showed a dynamic subcellular distribution indistinguishable from EGFP-Myo9b (Figure 2), but did not induce any obvious morphological changes, we used EGFP-Myo9b^{GAP-} constructs for our subsequent studies. The EGFP-Myo9b^{GAP-} fusion protein was enriched in extending lamellipodia, membrane ruffles, and occasionally at filopodial tips, the regions of active F-actin polymerization (Figure 2; Supplementary Video 1). The increased fluorescence intensity in these dynamic regions was not attributable to differences in cell thickness as revealed by TIRF-microscopy that illuminates a thin optical layer near the cover glass surface of ~100 nm (Figure 2, A, C, and E). A comparable localization was observed for Myo9b^{GAP-} that was fused C-terminally to EGFP and for endogenous Myo9b that was visualized by indirect immunofluorescence (data not shown). The tail of Myo9b can be alternatively spliced at the C-terminus extending it by 137 amino acids (Grewal *et al.*, 1999). This longer splice form of Myo9b showed the same subcellular distribution as the shorter isoform and hence no subcellular targeting information appeared to be encoded in the C-terminal extension (Figure 2E).

Myo9b Is Targeted to Regions of Newly Polymerizing F-Actin by Its Motor Activity

Next, we investigated how Myo9b becomes targeted to regions of active actin polymerization. To test if a functional motor domain is needed, we introduced various mutations in the Myo9b motor domain to impair motor activity in

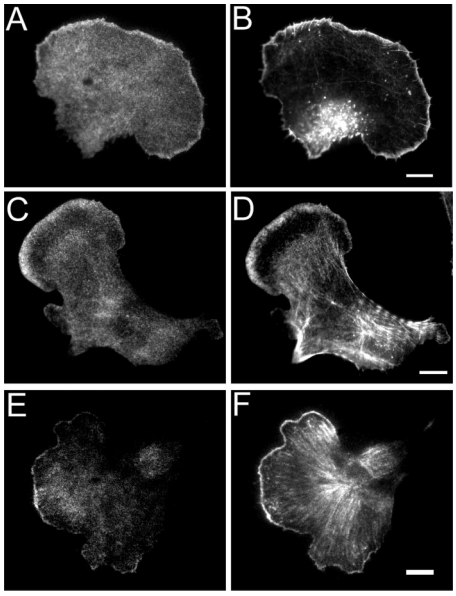

Figure 2. Myo9b is recruited to extending lamellipodia. B16/F1 cells were transfected with EGFP-Myo9b (A and B), EGFP-Myo9b^{GAP-} (C and D), or EGFP-Myo9b$^{C\text{-}alt}$ (E and F), replated on laminin-coated coverslips, and fixed and permeabilized as described in *Materials and Methods.* F-actin was labeled with Alexa 594–conjugated phalloidin. Left panels, TIRF-M images of EGFP-Myo 9b, EGFP-Myo9b $^{GAP-}$, and EGFP-Myo9b$^{C\text{-}alt}$ 1 (A, C, and E); right panels, the corresponding F-actin staining (B, D, and F). Scale bars, 10 μm.

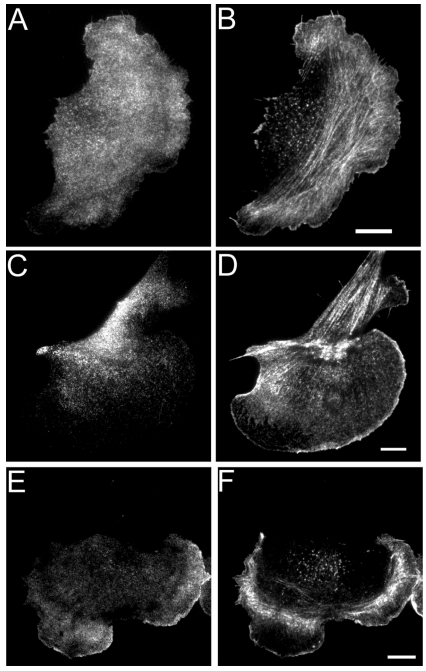

Figure 3. A functional motor domain is necessary for Myo9b targeting to extending lamellipodia. B16/F1 cells were transfected with different EGFP-Myo9b constructs, fixed, and labeled with Alexa 594–conjugated phalloidin. TIRF-M images of cells expressing either EGFP-Myo9b$^{G244R/GAP-}$ (A), EGFP-Myo 9b$^{R295C/GAP-}$ (C), or Myo 9b$^{ext-/GAP-}$-EGFP (E) are shown together with their corresponding F-actin staining (B, D, and F). Scale bars, 10 μm.

different ways. A point mutation was introduced into the nucleotide-binding P-loop (G244R; Myo9b^{G244R}) that is predicted to abolish nucleotide-binding (Bejsovec and Anderson, 1990) and block the chemomechanical cycling of Myo9b in the nucleotide-free state. The myosin nucleotide-free state typically has a high affinity for F-actin. Another point mutation (R295C; Myo9b^{R295C}) introduced in Myo9b is predicted to abolish ATP hydrolysis as the same mutation in *Dictyostelium discoideum* myosin II blocked ATP hydrolysis (Shimada *et al.*, 1997). The analogous mutation in human myosin VIIA has been found to cause Usher syndrome type IB (Weil *et al.*, 1995). Myosins in the ATP-bound state generally have a weak affinity for F-actin. However, Myo9b in the ATP-bound state can interconvert between a form of weak and strong actin affinity in vitro (Nalavadi *et al.*, 2005). Unlike Myo9b, both Myo9b motor domain point mutants, EGFP-Myo9b$^{G244R/GAP-}$ and EGFP-Myo9b$^{R295C/GAP-}$ did not show an obvious accumulation in extending lamellipodia, membrane ruffles and filopodia as no increased fluorescence intensity was observed in these cellular regions (Figure 3, A–D). This result indicates that a functional motor domain that can cycle between different nucleotide binding states is necessary for Myo9b targeting to regions of active actin filament polymerization.

To analyze whether a functional motor domain is not only necessary for directing the dynamic subcellular targeting of Myo9b, but also sufficient, we expressed a recombinant Myo9b motor domain, encompassing the head region and the light chain binding domain (Myo9b-head-LCBD). The subcellular distribution of EGFP-Myo9b-head-LCBD was very similar to that of the full-length Myo 9b (Figure 4, A and B). It was enriched in extending lamellipodia and circular actin clouds, the regions of active actin polymerization. The tail domain of Myo9b^{GAP-} (amino acids 1053–1980) lacking the motor domain appeared evenly distributed in the cytosol and the cell membrane (Figure 4, C and D). In conclusion, the motor domain is both necessary and sufficient for the correct subcellular targeting of Myo9b to regions of active actin polymerization.

Little is known about the functions of two regions in the Myo9b motor domain that are specific to class IX myosins.

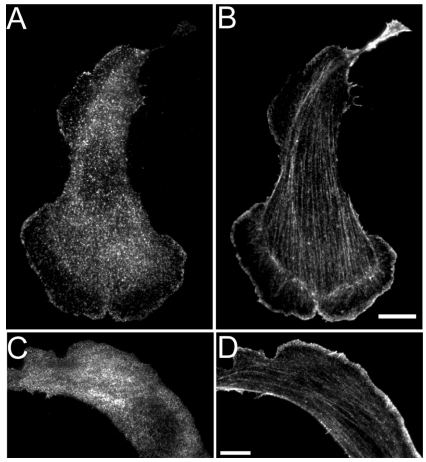

Figure 4. A functional motor region is sufficient for targeting of Myo9b to extending lamellipodia. B16/F1 cells were transiently transfected with EGFP-Myo9b-head-LCBD (A) and EGFP-Myo9b-tail^{GAP-} (C), fixed and labeled with Alexa 594–conjugated phalloidin (B and D), and subsequently analyzed by TIRF microscopy. Scale bars, 10 μm.

Deletion of the myosin class IX-specific region N-terminal to the Myo9b motor domain (referred to as extension; Myo9b^{ext-}) results in altered binding of nucleotide and F-actin and in altered coupling between the two sites (Nalavadi *et al.*, 2005). The expression of a Myo9b$^{ext-/GAP-}$-EGFP construct revealed that its proper targeting to regions of active actin polymerization was still occurring (Figure 3, E and F), but targeting appeared frequently diminished, implicating that the class IX–specific N-terminal motor extension influences the Myo9b motor properties needed for proper subcellular targeting.

In its myosin head domain Myo9b contains a large insertion that has been proposed to be critical for processive movement (Nishikawa *et al.*, 2006). This insertion can be alternatively spliced and has a length of 140–175 amino acids (Nalavadi *et al.*, 2005). It is inserted at loop 2 (50/20-kDa junction), a loop implicated in controlling actin affinity (Furch *et al.*, 1998; Murphy and Spudich, 1999; Joel *et al.*, 2001; Yengo and Sweeney, 2004; Krementsova *et al.*, 2006). Deletion of this insertion decreased the affinity of Myo9b for actin in all nucleotide states about 4-fold and reduced the nucleotide affinity to acto-Myo9b more than 10-fold (Nalavadi *et al.*, 2005). EGFP-Myo9b^{GAP-} that had this insertion at loop 2 deleted (EGFP-Myo9b$^{ins-/GAP-}$) failed to accumulate in extending lamellipodia and membrane ruffles (Figure 5, A and B). However, EGFP-Myo9b$^{ins-/GAP-}$ showed a more prominent accumulation at the tips of filopodia and retracting cell extensions (Figure 5, A–C, arrowheads in A–C; Supplementary Video 2). A quantitative analysis revealed that cells expressing EGFP-Myo9b$^{ins-/GAP-}$ did not form more extensions per millimeter of cell perimeter than did cells expressing EGFP-Myo9b^{GAP-} or EGFP, but that the number of extensions that showed bright fluorescence at their tips was significantly increased from 6.47% in cells transfected with EGFP-Myo9b^{GAP-} to 30.08% in cells transfected with EGFP-Myo9b$^{ins-/GAP-}$ (Figure 6). EGFP alone did not accumulate at the tips of thin cell extensions. To investigate whether altered Myo9b motor properties are responsible for the enhanced targeting of the Myo9b$^{ins-/GAP-}$ to the tips of thin cell extensions, we transfected cells with an EGFP-Myo9b-head-LCBD^{ins-} construct. The Myo9b motor region that had the insertion at loop 2 deleted, failed to localize to the tips of thin extensions (Figure 5, D and E), and did not accumulate in protruding lamellipodia (Figure 5, D and E). This result suggests that the tail region is necessary for the enrichment in the tips of filopodia and retraction fibers. However, the tail region is not sufficient because the tail region alone did not localize to the tips of filopodia and retraction fibers. Therefore, additional elements within the motor region must contribute to the tip localization. A pair of lysine residues located in the C-terminal end of loop 2 of smooth muscle myosin II and myosin Va has been shown to be responsible for high actin affinity (Joel *et al.*, 2001; Yengo and Sweeney, 2004). C-terminal to the loop 2 insertion, Myo9b contains four lysine residues. These four lysine residues were exchanged to alanine residues in a construct lacking the insertion (Myo9b$^{ins-4A/GAP-}$) to analyze a possible contribution of these residues to the subcellular localization of Myo9b. This construct also failed to accumulate at regions of active actin polymerization and in addition no longer accumulated at the tips of filopodia or retraction fibers (Figure 5, F and G, arrowheads). These results reveal a cooperative function of the Myo9b tail region and the four lysine residues following the loop 2 insertion in localizing Myo9b to the tips of filopodia and retraction fibers. The Myo9b loop2 insertion has a crucial role in localizing Myo9b to protruding lamellipodia and membrane ruffles and modulates the targeting to the tips of filopodia and retraction fibers.

The Exchange Rate of Myo9b in Lamellipodia Depends on the Turnover of F-Actin

To determine the in vivo dynamics of Myo9b in extending lamellipodia of B16/F1 cells, we performed FRAP experiments (Figures 7 and 8). The extension rates of the lamellipodia were significantly slower than the rates of the fluorescence recovery, so that for the duration of the FRAP experiments the changes in the area covered by a lamellipodium were negligible (<4%). Considering that the lamellipodium is limited by the plasma membrane at the leading edge and hence not equally accessible for unbleached molecules and that EGFP-Myo9b^{GAP-} is a motor expected to move not only by diffusion, a general kinetic model was applied to determine the mobile fraction and the rates of recovery. The obtained fluorescence recovery data (Figure 7) were fitted to Equation 1 (see *Materials and Methods*). In EGFP-Myo9b^{GAP-}–expressing cells, the fluorescence recovered homogeneously within the bleached area to about 86% within 30 s (Figure 7, A and B). The recovery data of the mobile fraction were best fitted with two kinetic components F1 and F2 and corresponding fast (t1) and slow (t2) recovery times. All parameters determined for the different constructs by FRAP experiments are shown in Table 1. For EGFP-Myo9b^{GAP-} the fast and slow components had recovery times of 0.69 and 13 s, respectively. The amplitude of the slow process was roughly double the amplitude for the fast process with F2 0.57 and F1 0.27 (Figure 8). Similar results were obtained with EYFP-Myo9b (Figure 8, A–C). EGFP-Myo9b^{GAP-} and EYFP-Myo9b are expected to interact with the dense network of actin filaments in lamellipodia and move (processively) either toward the plus- or minus-ends of the dynamic actin filaments. Therefore, we compared its kinetics with those of actin by performing FRAP experiments in cells transfected with EGFP-actin. As observed previously, recovery of the actin fluorescence started at the leading edge, moving gradually inward until the entire lamellipodium was labeled homogeneously again (Figure 7A). Quantitative analysis of the obtained FRAP data revealed a mobile fraction of 82% with double the molecules moving with the slow time constant (F2 0.57) than with the fast time constant (F1 0.25) and recovery times of t1 = 0.64 s and t2 = 13.6 s, values remarkably similar to those obtained with EGFP-Myo9b^{GAP-} and EYFP-Myo9b (Figure 8, A–C). To test if the turnover kinetics of Myo9b in the lamellipodium is dependent on the turnover of actin, we treated cells with jasplakinolide, which inhibits actin-filament disassembly. Treatment of cells with jasplakinolide that prevented the recovery of actin fluorescence after photobleaching (Supplementary Figure S2) resulted in faster turnover kinetics of EGFP-Myo9b^{GAP-} (Figure 8F). It exhibited a significantly larger fraction of fast-moving molecules (F1 0.71) and a significantly smaller fraction of slow-moving molecules (F2 0.27). The slow time constant t2 was significantly faster (7.36 s), whereas the fast time constant t1 was somewhat increased (1.43 s). In cells transfected with EGFP alone, the fluorescence recovery was clearly distinct (Figure 8, A–C). The recovery of EGFP fluorescence was more complete, approaching a mobile fraction of almost 100%, and the recovery was clearly much faster with t1 of 0.29 s and t2 of 1.76 s, respectively. The slow time constant t2 of EGFP differed significantly from t2 of the Myo9b and actin constructs. The amplitudes of the fast- and slow-moving EGFP molecules were reversed in comparison to EGFP-Myo9b^{GAP-} and actin with a higher proportion of the EGFP molecules moving with t1 (Figure 8, B and C).

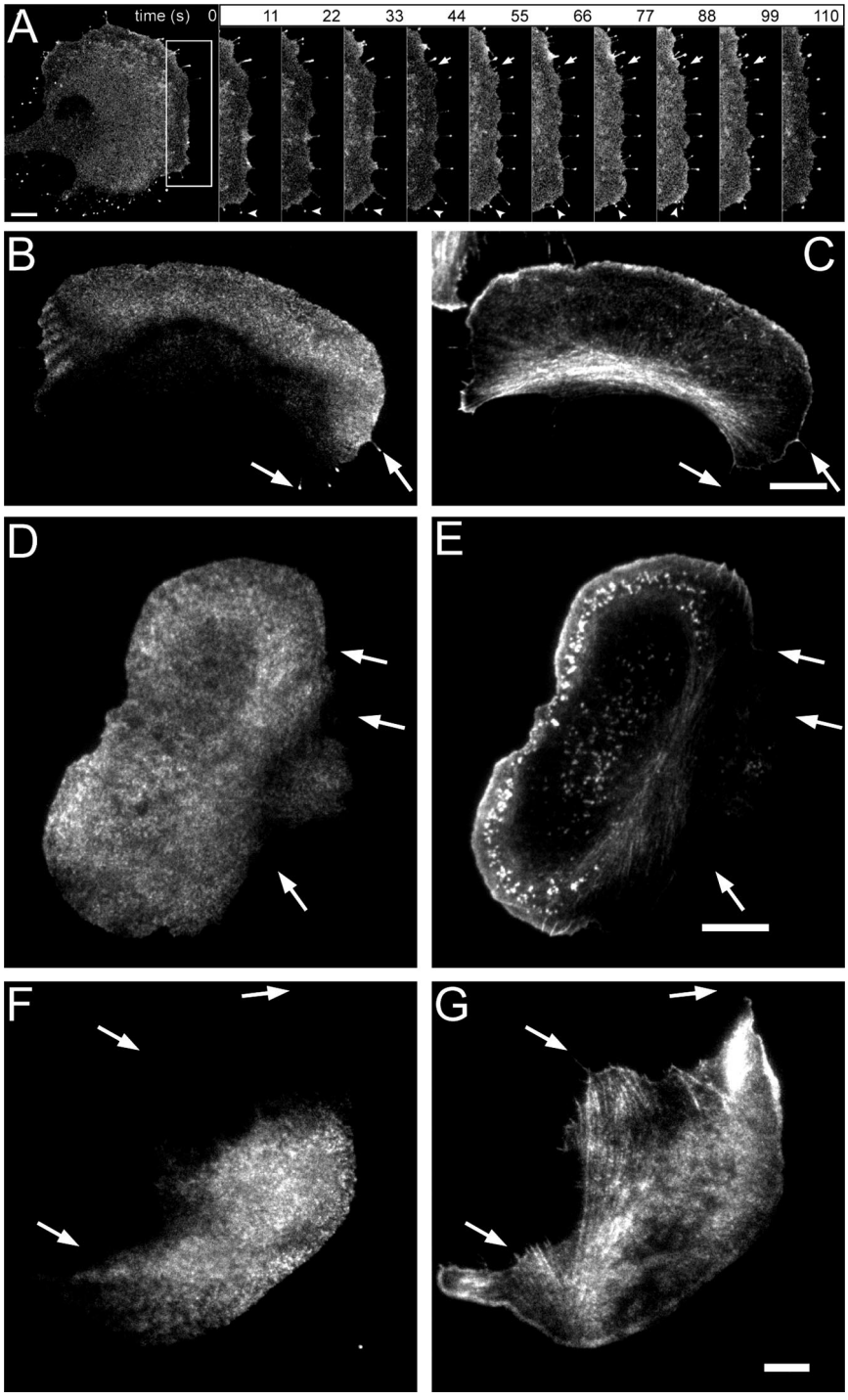

Figure 5. EGFP-Myo9b$^{ins-/GAP-}$ accumulates at the tips of filopodia and retraction fibers, but not in extending lamellipodia. EGFP-Myo9b-head-LCBD^{ins-} and EGFP-Myo9b$^{ins-4A/GAP-}$ accumulate in neither region. B16/F1 cells were transfected with EGFP-Myo9b$^{ins-/GAP-}$, EGFP-Myo9b-head-LCBD^{ins-}, or EGFP-Myo9b$^{ins-4A/GAP-}$. (A) Confocal time series of a living B16/F1 cell expressing EGFP-Myo9b$^{ins-/GAP-}$. Bright fluorescent puncta were detected at the tips of protruding (arrows) as well as retracting filopodia (arrowheads; Supplementary Video 2). (B and C) A fixed cell expressing EGFP-Myo9b$^{ins-/GAP-}$ was analyzed for EGFP fluorescence (B) and F-actin (C) by TIRF microscopy. Arrowheads point at tips of cellular extensions. (D and E) A fixed cell transfected with EGFP-Myo9b-head-LCBD^{ins-} was analyzed for EGFP fluorescence (D) and F-actin (E) by TIRF microscopy. Deletion of the tail region abolished the accumulation at the tips of cell extensions completely (arrowheads in D and E). (F and G) A fixed cell expressing EGFP-Myo9b$^{ins-4A/GAP-}$ was analyzed for EGFP (F) and F-actin (G) distribution by TIRF microscopy. No accumulation of this construct at tips of cellular extensions was detected (arrowheads in F and G). Scale bars, 10 μm.

The Motor Region of Myo9b Is a Major Determinant for the Turnover Kinetics of Myo9b in the Lamellipodium

A functional Myo9b motor domain was both necessary and sufficient for directing Myo9b to extending lamellipodia, suggesting that its kinetics in the lamellipodium could be determined largely by the motor properties. The EGFP-Myo9b-head-LCBD protein demonstrated recovery kinetics after photobleaching similar to EGFP-Myo9b^{GAP-} (Figure 8, D–F). No significant difference in the time constants of recovery or the amplitudes was noticed, indicating that the motor region is determining the exchange kinetics in the lamellipodium. The EGFP-Myo9b-tail^{GAP-} protein that has the head-LCBD (motor) region deleted was not enriched in extending lamellipodia. The fluorescence recovery for this construct was faster than for EGFP-Myo9b^{GAP-} and -head-LCBD constructs (Figure 8, D–F). Specifically, the time constant of slow recovery t2 was significantly faster for EGFP-Myo9b-tail^{GAP-} (t2 5.3 s) than for EGFP-Myo9b^{GAP-} or EGFP-Myo9b-head-LCBD (t2 11.5–13.6 s). These results indicate that the tail of Myo9b is exchanging faster than Myo9b and the Myo9b motor region. However, it exchanges still considerably slower than EGFP.

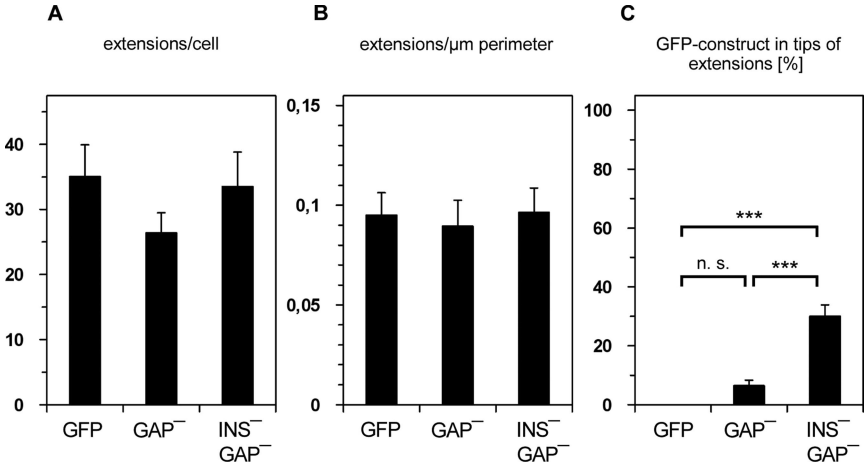

Figure 6. EGFP-Myo9b$^{ins-/GAP-}$ accumulates more often at the tips of cell extensions than EGFP-Myo9b^{GAP-}. (A) Cell extensions were quantified in B16/F1 cells expressing EGFP alone (15 cells), EGFP-Myo9b^{GAP-} (17 cells), and EGFP-Myo9b$^{ins-/GAP-}$ (15 cells). (B) The number of extensions per micrometer perimeter does not differ significantly in cells expressing EGFP (0.1 ± 0.01), EGFP-Myo9b^{GAP-} (0.09 ± 0.01), or EGFP-Myo9b$^{ins-/GAP-}$ (0.1 ± 0.01). (C) An increased number of cell extensions showing an accumulation of EGFP fluorescence at their tips was noticed in cells transfected with EGFP-Myo9b$^{ins-/GAP-}$ (30.08%) in comparison to cells transfected with EGFP-Myo9b^{GAP-} (6.47%) or EGFP (0%), respectively. *** Values that differ significantly from each other ($p < 0.001$); n.s., values that do not differ significantly from each other; error bars, SEM.

The Exchange Rate of Myo9b in the Lamellipodium Is Influenced by Its Motor Activity

Next, we determined whether the motor activity of Myo9b is affecting its exchange rate in the lamellipodium. Introduction of point mutations that presumably arrest the ATPase cycle in Myo9b either at the nucleotide binding or ATP hydrolysis step led to significant changes in the kinetic parameters as determined by FRAP. Both of these two different point mutations led to an increase in the immobile fraction by 10–15% and a reduction in the amplitude of F2 by ~35%. The time constants of the slow recovery t2 were for both mutants significantly faster than for EGFP-Myo9b^{GAP-} with a t2 for the EGFP-Myo9b$^{G244R/GAP-}$ mutant of 7.6 s and for the EGFP-Myo9b$^{R295C/GAP-}$ mutant of 6.8 s, respectively. In comparison to EGFP-Myo9b^{GAP-} and EGFP-Myo9b$^{G244R/GAP-}$, the time constant of fast recovery for the EGFP-Myo9b$^{R295C/GAP-}$ mutant (t1 = 0.36 s) was significantly faster (Figure 8, G–I), suggesting that the interaction with actin is also contributing somewhat to t1. These differences in the exchange rates for the two mutants are in accordance with their altered subcellular distributions and underscore the assumption that the mutations do affect the chemomechanical cycle. These data show that the motor activity of Myo9b contributes significantly to the exchange rates in the lamellipodium.

The large insertion at loop 2 of the Myo9b head has been proposed to act as an actin tether and thereby affect motor properties. Indeed, deletion of amino acids 681–820 of the extended loop 2 altered its turnover kinetics (Figure 8, D–F). The time constant of slow recovery t2 was significantly faster with 8.3 s for EGFP-Myo9b$^{ins-/GAP-}$ than for EGFP-Myo9b^{GAP-}, and the amplitudes were similar to those of the constructs carrying a point mutation in the head domain. These data demonstrate that removal of the loop 2 insertion influences the turnover kinetics in accordance with the altered localization.

The Turnover Kinetics of PAGFP-Myo9b Constructs in the Lamellipodium as Determined by Photoactivation

To monitor the in vivo turnover kinetics of Myo9b at the lamellipodium in a more direct way, we performed photoactivation experiments with B16/F1 cells expressing either PAGFP, PAGFP-actin, and different PAGFP-Myo9b fusion proteins. As in the FRAP experiments, photoactivation was performed in a narrow region in the actin-rich zone at the front of protruding lamellipodia that was monitored by the fluorescence of cotransfected mRFP-actin. Irradiation of the ROI with 405-nm laser light led to a rapid initial increase of fluorescence intensity within the ROI that was followed by a decrease in fluorescence intensity over time (Figure 9, A and B). This decrease was fitted to a biexponential kinetic model (Equation 2; Figure 9C). The protrusion of lamellipodia in the initially activated ROI during the time course of an experiment was considered to be negligible. All parameters determined for the different constructs by photoactivation experiments are summarized in Table 1.

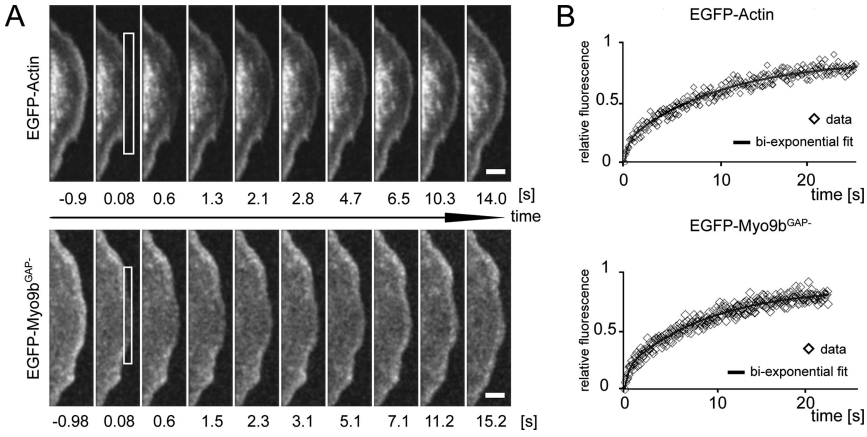

Figure 7. The exchange of Myo9b inside the lamellipodia of living cells is similar to the dynamics of actin and dependent on a functional motor domain. (A) Fluorescence images of a bleaching experiment with EGFP-actin and EGFP-Myo9b^{GAP-}, respectively (bar, 5 μm). The first image shows the lamellipodia before bleaching. EGFP-actin clearly recovers starting from the leading edge, whereas EGFP-Myo9b^{GAP-} recovers homogenously. The white rectangle indicates the region that was bleached and used for fluorescence intensity determination. (B) Normalized recovery kinetics (◇) of the experiments shown in A. The continuous curves demonstrate the fit results obtained with the biexponential fit function (Equation 1).

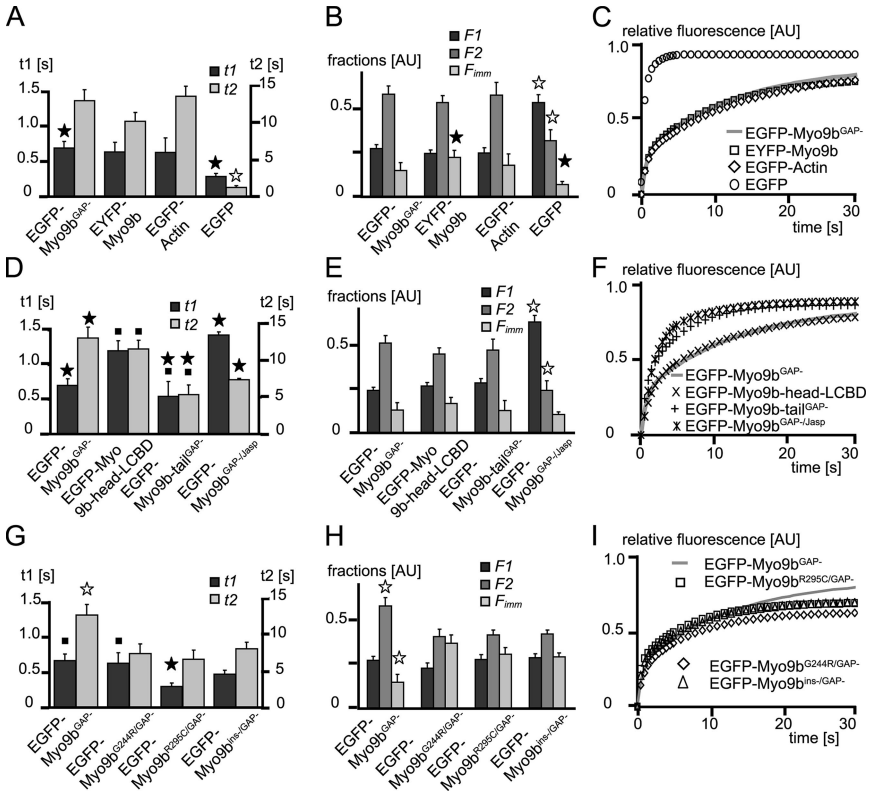

Figure 8. Turnover kinetics of EGFP-Myo9b^{GAP-}, EGFP, EGFP-actin, and EGFP-Myo9b-mutants in lamellipodia. Bar diagrams of calculated fast (t1) and slow (t2) time constants (A, D, and G), the corresponding mobile (F1, F2) and immobile (F_{imm}) fractions (B, E, and H), and curves of the recovery kinetics calculated from the average values (C, F, and I) are shown for the different proteins tested in the FRAP experiments. Left, time scale for t1; right, the time scale for t2 (A, D, and G). The bleached fraction normalized to 1 is represented by the fast-recovering fraction (F1), the slow-recovering fraction (F2), and the immobile fraction (F_{imm}; B, E, and H). The respective constructs are indicated. (A) The t2, F1, and F2 values for EGFP (☆ in A and B) differ significantly from the respective values of EGFP-Myo9b^{GAP-}, EGFP-actin, and EYFP-Myo9b. The constant t1 of EGFP differed from the value of EGFP-Myo9b^{GAP-} only (bars marked with a ★ in A). F_{imm} of EGFP differs significantly from F_{imm} of EYFP-Myo9b (bars marked with a filled star in B). The recovery curves shown in C demonstrate a high similarity between EGFP-Myo9b^{GAP-}, EGFP-actin, and EYFP-Myo9b. The comparison of EGFP-Myo9b^{GAP-} with EGFP-Myo9b-head-LCBD and EGFP-Myo9b-tail in D–F reveals that the motor domain is essential for the intracellular Myo9b exchange kinetics. Treatment of cells with 1 μM jasplakinolide (Jasp) demonstrates that the EGFP-Myo9b^{GAP-} turnover kinetics are dependent on the kinetics of the actin turnover. The tail region and in cells treated with jasplakinolide EGFP-Myo9b^{GAP-} (EGFP-Myo9b$^{GAP-/Jasp}$) exchange significantly faster, and t2 is significantly smaller for EGFP-Myo9b-tail and EGFP-Myo9b$^{GAP-/Jasp}$ than for Myo9b^{GAP-} (D, ★). t2 of EGFP-Myo9b-tail^{GAP-} was significantly faster than for EGFP-Myo9b-head-LCBD (■). The t1 of EGFP-Myo9b-tail^{GAP-} is significantly smaller than t1 of the EGFP-Myo9b-head-LCBD only (■). EGFP-Myo9b^{GAP-} exhibits after treatment of cells with jasplakinolide a significantly slower t1 than EGFP-Myo9b^{GAP-} and EGFP-Myo9b-tail^{GAP-} (★). The mobile fractions F1 and F2 of EGFP-Myo9b^{GAP-} in cells treated with jasplakinolide are significantly different from the others (☆). The recovery curves clearly show the faster exchange of the EGFP-Myo9b-tail and EGFP-Myo9b$^{GAP-/Jasp}$ (F). Myo9b motor domain mutants exhibit a significantly shorter t2 than that of EGFP-Myo9b^{GAP-} (G, ☆), an increase of the immobile fraction and a significant decrease of the slow fraction (H, ☆). The short time constant t1 differs significantly between EGFP-Myo9b$^{R295C/GAP-}$ on the one hand (G, ★) and EGFP-Myo9b^{GAP-} and EGFP-Myo9b$^{G244R/GAP-}$on the other (G, ■). The kinetic curves reflect the bigger immobile fraction, and the faster recovery kinetics of the mutants with compromised motor activity (I).

First, we determined the kinetics of PAGFP in the lamellipodium of transfected B16/F1 cells. PAGFP was exchanging rapidly with a fast time constant t1 of 0.26 s and a t2 of 1.74 s (Figure 10A). The mobile fraction represented 94% and the amplitude for the fast exchanging molecules was significantly higher than the amplitude for the slow exchanging fraction as expected for a predominantly freely diffusing protein (Figure 10B).

PAGFP fused to actin revealed a mobile fraction of 82% that exhibited significantly slower turnover kinetics than PAGFP alone with a t1 = 2.77 s and t2 = 12.18 s (Figure 10A). A significant fraction of photoactivated PAGFP-actin molecules are expected to be constituents of actin filaments and exchange with the rate of actin filament treadmilling. Therefore, the time constant t2 represents the average turnover rate of actin filaments in the lamellipodium. The relationship of the amplitudes for the fast and slow subpopulations of PAGFP-actin was essentially reversed in comparison to that of PAGFP with the majority of PAGFP-actin molecules (F2 = 0.59) exchanging with the slow time constant (Figure 10B).

The analysis of photoactivated PAGFP-Myo9b^{GAP-} in the lamellipodium revealed turnover kinetics very similar to those of PAGFP-actin. The slow time constant t2 with 11.38 s was comparable to that of F-actin (Figure 10A). The fast exchanging fraction of PAGFP-Myo9b^{GAP-} showed a time constant t1 of 0.99 s that was 2–3-fold faster than the fast exchanging fraction of PAGFP-actin. Given the relatively large difference in size of the two molecules, one would expect a slower time constant for PAGFP-Myo 9b^{GAP-} than for PAGFP-actin, if t1 would represent mostly diffusion of single molecules. The reason for this difference is not known. The mobile fraction of PAGFP-Myo9b^{GAP-} represented 92% of all molecules. As with PAGFP-actin, the majority of the mobile molecules of PAGFP-Myo9b^{GAP-} were moving with the slower time constant t2, but the difference between F1 and F2 was less pronounced (Figure 10B).

The Myo9b motor region including the light-chain binding domain fused N-terminally to PAGFP showed dynamics strikingly similar to that of PAGFP-Myo9b^{GAP-} and PAGFP-actin (Figures 9C and 10A), confirming that the motor domain is a major determinant for the observed dynamics of Myo9b in the lamellipodium. The slow time constant t2 of PAGFP-Myo9b-head-LCBD was 11.36 s. This t2 value is very similar to the t2 values determined for PAGFP-actin and PAGFP-Myo9b^{GAP-}. The fast time constant t1 = 1.03 s was similar to that of PAGFP-Myo9b^{GAP-}. Interestingly, the relationship of the amplitudes of both processes was reversed in comparison to the amplitudes of the Myo9b full length and the actin construct. The amplitude of photoactivated Myo9b-head-LCBD proteins exchanging with the time constant t1 was 48% and that exchanging with the time

Table 1. FRAP and photoactivation data summary

Construct	PA	FRAP	PA	FRAP	PA	FRAP	PA	FRAP	PA	FRAP	PA	FRAP
	t1 [s]	t1 [s]	t2 [s]	t2 [s]	F1	F1	F2	F2	F_{imm}	F_{imm}	N	N
(PA)/(E)GFP	0.26 ± 0.07	0.29 ± 0.05	1.74 ± 0.91	1.30 ± 0.20	0.59 ± 0.04	0.53 ± 0.04	0.26 ± 0.04	0.32 ± 0.06	0.16 ± 0.02	0.07 ± 0.02	14	20
(PA)/(E)GFP-actin	2.77 ± 0.56	0.64 ± 0.20	12.18 ± 2.95	13.60 ± 1.30	0.33 ± 0.03	0.25 ± 0.03	0.59 ± 0.04	0.57 ± 0.07	0.03 ± 0.01	0.18 ± 0.07	20	21
EYFP-Myo9b	nd	0.64 ± 0.14	nd	10.20 ± 1.20	nd	0.24 ± 0.02	nd	0.53 ± 0.04	nd	0.22 ± 0.04	nd	20
(PA)/(E)GFP-Myo9b^{GAP-}	0.99 ± 0.23	0.69 ± 0.10	11.38 ± 3.22	13.00 ± 1.50	0.37 ± 0.02	0.27 ± 0.02	0.49 ± 0.03	0.57 ± 0.05	0.08 ± 0.03	0.14 ± 0.05	9	28
EGFP-Myo9b^{GAP-}+jasp	nd	1.43 ± 0.35	nd	7.36 ± 2.96	nd	0.71 ± 0.09	nd	0.27 ± 0.04	nd	0.12 ± 0.04	nd	17
(PA)/(E)GFP-Myo9b-headLCBD	1.03 ± 0.26	1.2 ± 0.40	11.36 ± 3.99	11.50 ± 2.40	0.48 ± 0.06	0.30 ± 0.03	0.35 ± 0.04	0.51 ± 0.06	0.11 ± 0.05	0.19 ± 0.06	7	17
(PA)/(E)GFP-Myo9b-tail^{GAP-}	0.85 ± 0.17	0.55 ± 0.06	4.29 ± 0.87	5.30 ± 0.40	0.42 ± 0.06	0.32 ± 0.02	0.39 ± 0.06	0.53 ± 0.03	0.07 ± 0.01	0.14 ± 0.03	9	19
EGFP-Myo9b$^{G244R/GAP-}$	nd	0.66 ± 0.16	nd	7.60 ± 1.40	nd	0.23 ± 0.03	nd	0.40 ± 0.04	nd	0.36 ± 0.05	nd	20
EGFP-Myo9b$^{R295C/GAP-}$	nd	0.36 ± 0.05	nd	6.80 ± 1.30	nd	0.28 ± 0.03	nd	0.42 ± 0.03	nd	0.31 ± 0.04	nd	19
EGFP-Myo9b$^{ins-/GAP-}$	nd	0.50 ± 0.06	nd	8.30 ± 1.00	nd	0.29 ± 0.02	nd	0.42 ± 0.02	nd	0.29 ± 0.02	nd	27

PA, photoactivation; nd, not determined.

constant t2 35% (Figure 10B). The fraction of immobile molecules was 11% (Figure 10B).

The tail construct PAGFP-Myo9b-tail^{GAP-} exhibited a faster turnover rate in comparison to the other investigated PAGFP fusion proteins. The determined time constant of the slow dynamic process t2 of PAGFP-Myo9b-tail^{GAP-} was 4.29 s, and the fast time constant t1 was 0.85 s, respectively (Figure 10A). These time constants are both faster than the time constants of the other PAGFP-Myo9b constructs and PAGFP-actin, but slower than the time constants obtained with PAGFP alone (Figure 10A). The mobile fraction was 93% with roughly equal amplitudes for the fast- and slow-exchanging molecules (Figure 10B). In conclusion, these results suggest that the Myo9b-tail^{GAP-} domain is not diffusing like PAGFP (possibly because of an interaction with Rho), but that it is also not coupled to the dynamics of actin in the lamellipodium.

DISCUSSION

In the present study we show that the class IX myosin-RhoGAP Myo9b accumulates in regions of active actin polymerization such as extending lamellipodia and ruffles. This accumulation is dependent on a functional motor domain that is also sufficient for proper targeting. The two class IX–specific regions in the myosin head of Myo9b and four lysine residues C-terminal of loop 2 are contributing to proper subcellular localization. The turnover kinetics of Myo9b in the lamellipodium is similar to that of actin, and it is accelerated when the disassembly of F-actin is inhibited. The motor region and its motor activity as well as the loop2 insertion are significantly contributing to the observed turnover kinetics of Myo9b in the lamellipodium.

Why is Myo9b accumulating at sites of actin polymerization? Unlike older actin filaments, newly polymerized F-actin is initially free of any other actin-binding proteins that might compete with Myo9b for binding. Alternatively, the single-headed processive Myo9b might easily dissociate when tripping over other actin-binding proteins associated with older actin filaments. On directed movement toward the plus- or minus-ends of actin filaments, it may accumulate visibly in regions of abundant actin filament ends such as lamellipodia, ruffles, and filopodia (only plus-ends). Another possibility is that Myo9b motor activity becomes locally activated at sites of actin polymerization by specific signaling molecules. However, at present nothing is known about the regulation of the Myo9b motor activity.

Point mutations analogous to mutations that block the ATPase cycle at two different steps in other myosins led to a loss of Myo9b accumulation in regions of actin polymerization. These results indicate that the introduced point mutations affect the ATPase cycle of Myo9b and that motor activity is essential for Myo9b localization. The myosin class IX–specific N-terminal extension to the head domain contributed to the proper subcellular localization. The slightly diminished localization of Myo9b after removal of the N-terminal extension is best explained by an alteration in Myo9b motor properties. In agreement with this notion, a recent biochemical characterization of a similar construct without EGFP demonstrated a significantly reduced actin affinity and an increased rate of nucleotide binding (Nalavadi *et al.*, 2005). The second class IX–specific region in the myosin head of Myo9b, the large insertion at loop 2, had been speculated to act as an actin tether that is necessary to allow for processive movement of Myo9b (Inoue *et al.*, 2002; Post *et al.*, 2002). However, relatively minor changes were observed in kinetic and actin-binding experiments in vitro upon removal of the loop 2

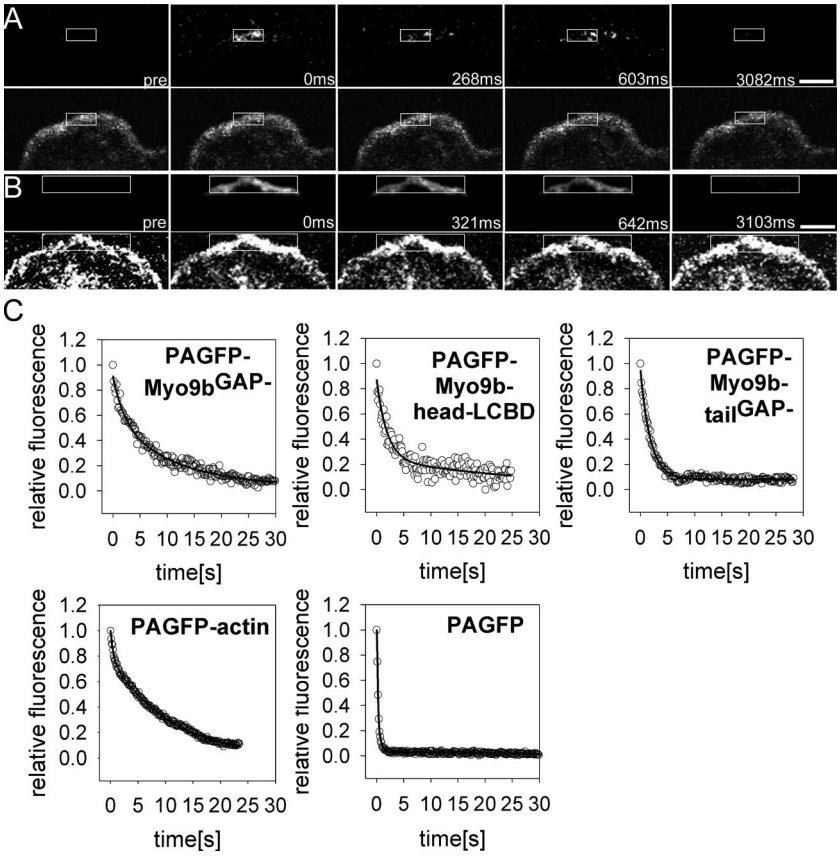

Figure 9. In lamellipodia the dynamics of Myo9b and Myo9b motor domain are similar to the dynamics of actin as determined by photoactivation experiments. (A) Time-lapse series of a photoactivation experiment in a B16/F1 cell double-transfected with PAGFP-Myo9b^{GAP-} and mRFP-actin. PAGFP was activated in a region of interest (white box) in the lamellipodium by a high-intensity laser pulse of 405 nm at time point t = 0 ms (second frame). Photoactivation led to a rapid increase in fluorescence intensity. The following decrease in fluorescence intensity in the ROI was monitored over time. Top row, PAGFP-Myo9b^{GAP-}; bottom row, mRFP-actin. Time points of the acquired images before or after photoactivation are indicated in the bottom panel. Scale bar, 5 μm. (B) Time-lapse series of a photoactivation experiment in a B16/F1 cell cotransfected with PAGFP-actin and mRFP-actin. Scale bar, 5 μm. (C) Representative determinations of PAGFP-fluorescence intensity decay in the ROI as a function of time after photoactivation. Individual experimental data of the fluorescence decay after photoactivation (○) and biexponential least-squares fits to the corresponding data points (black line) for PAGFP, PAGFP-actin, and the different photoactivatable Myo9b constructs (indicated above each trace) are shown. PAGFP shows the fastest kinetics, whereas PAGFP-actin, PAGFP-Myo9b^{GAP-}, and PAGFP-Myo9b-head-LCBD reveal similar kinetics. The tail construct PAGFP-Myo9b-tail^{GAP-} displays a recovery kinetic faster than the other Myo9b constructs and actin, but still slower than PAGFP alone.

insertion (Nalavadi *et al.*, 2005). Here we show that deletion of the loop 2 insertion accelerates the exchange rate in the lamellipodium and abolishes an accumulation in the lamellipodium. It remains to be seen if and how the loop 2 insertion affects processivity. Deletion of the loop 2 insertion revealed that the molecular mechanisms involved in localizing Myo9b in extending lamellipodia and ruffles differ from those that govern the accumulation in the tips of filopodia and retraction fibers. Four consecutive lysine residues located C-terminal to the loop 2 insertion and the tail region were both necessary for localizing Myo9b at the tips of filopodia and retraction fibers. Lysine residues at an analogous position in other myosins enhance the actin affinity (Joel *et al.*, 2001; Yengo and Sweeney, 2004). Therefore, it appears likely that these lysine residues control the localization of Myo9b in the tips of filopodia and retraction fibers through a modulation of the actin affinity of Myo9b. Additionally, the tail region either interacts with an unknown (membrane) component or modifies motor properties. The finding that the tail region exchanges much more slowly in the lamellipodium than EGFP supports the former possibility. Further support for the interaction of the tail region with an unknown component comes from the observation that deletion of the loop 2 insertion enhances the enrichment in the tips of filopodia and retraction fibers. This observation is best explained by an inhibitory constraint of the loop 2 insertion on the tail region. However, the interaction of the tail region with an unknown component alone is not sufficient for an enrichment at the tips of filopodia and retraction fibers as the tail region alone was not enriched there.

FRAP and photoactivation experiments were performed to determine the dynamics of Myo9b and different Myo9b constructs in lamellipodia. Inside lamellipodia the exchange of the molecular motor proteins observed was considered to be dependent on hindered diffusion (Potma *et al.*, 2001) superimposed by the interaction with a dense actin meshwork and the limiting plasma membrane. Therefore, we used a general kinetic model to characterize the fluorescence intensity kinetics after the bleach and activation pulses with three different fractions (Tyska and Mooseker, 2002). The results obtained by the two different experimental methods were generally in good agreement with each other.

The factors that influence time constants and amplitudes of those fractions can be delineated as follows. The fast time constant of recovery or decay, respectively, is dominated by diffusion that is dependent on the hydrodynamic radius of the molecules. In FRAP experiments performed in microvilli with actin and myosin 1a, the fast time constants were considerably slower and correlated with the molecular mass of the myosin Myo1A, its tail region, and actin (Tyska and Mooseker, 2002). Although the fast time constants in our study were comparable in the photoactivation and FRAP experiments and EGFP was faster than all the analyzed fusion proteins, no strict correlation existed between the fast time constant and the molecular mass of the analyzed molecule. Specifically, the fast time constants of the head-LCBD and the mutant R295C constructs did not conform to their molecular mass compared with the other constructs. This may indicate that the hydrodynamic radius is not strictly correlated to the molecular mass of the fusion proteins, that some of the fusion proteins form stable protein complexes, or most likely that some fast time constants have larger contributions of factors other than diffusion.

The slow time constant is likely to have contributions from hindered diffusion, actin binding and unbinding, directed movement, actin polymerization, and interactions

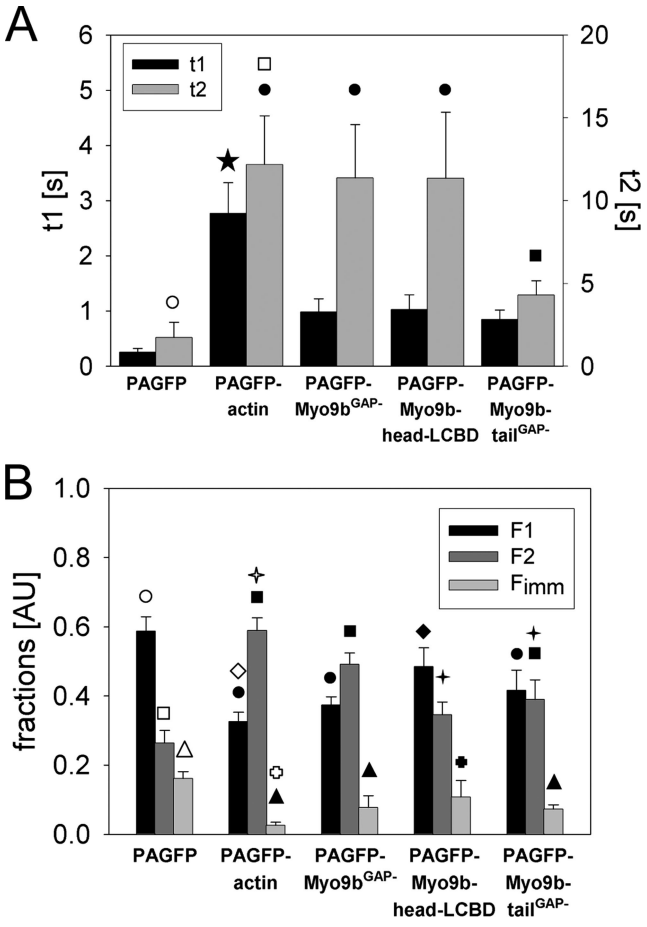

Figure 10. Kinetics of different PAGFP-constructs in the lamellipodium as determined by photoactivation. (A) Comparison of the time constants t1 and t2 derived for the different indicated photoactivatable constructs. A fast (t1, ■, left *y*-axis) and a slow (t2, ▨, right *y*-axis) time constant were calculated from the biexponential fits for each photoactivatable construct. Mean values ± SEM are given, and values indicated by a filled symbol differ significantly from values marked by the same open symbol above the bars. The filled star indicates that this value differs significantly from the values of all other constructs. (B) Comparison of the two amplitudes of the mobile fractions exchanging with the fast (t1) and slow (t2) time constants (F1, black; F2, gray) and the immobile fractions (F_{imm}, light gray) for the different indicated photoactivatable constructs derived from the biexponential fits to the fluorescence decay. Values that differ significantly from each other are indicated by open and closed symbols above the bars.

with other partners. The Myo9b motor region contributes significantly to the slow time constant as determined by expressing this region separately and by mutations that affect motor properties. The active and cycling Myo9b and truncated Myo9b-head-LCBD demonstrated the largest slow time constant. Both these two constructs exhibited comparable values for the slow time constant. The tail region exhibited a significantly faster slow exchange time. These results show that the slow exchange rate is dominated by interactions of the Myo9b motor region with F-actin. The mobile fraction of Myo9b blocked either in hydrolysis, or more noteworthy, in nucleotide binding, exchanged significantly faster. Both of these two Myo9b point mutants demonstrated an increased immobile fraction reflecting their inability to cycle. The faster exchange rate (~3–6 s) of the remaining mobile fraction of Myo9b molecules lacking motor activity and exchanging with the slow time constant suggests that they bound actin only weakly because the tail region had an even faster slow time constant. Myo9b that had the loop 2 insertion deleted had a slow time constant that was intermediate of Myo9b molecules with an intact or dead motor region, demonstrating that the loop 2 insertion influences motor properties.

Myo9b seems to exchange throughout lamellipodia evenly and with a similar slow time constant as actin. Although actin polymerization is promoted within the lamellipodium tip, most of the actin filaments in the lamellipodium are generated by basal polymerization and depolymerization throughout lamellipodia (Watanabe and Mitchison, 2002). The Myo9b exchange rate in the lamellipodium is dependent on the dynamics of the actin network. It is accelerated when the disassembly of F-actin is inhibited with jasplakinolide. This is in accordance with the lack of a prominent association of Myo9b with older and more static actin filament arrays in cells. This observation might be explained by competition with other actin-binding proteins or a lack of Myo9b activating signals that are coupled with actin polymerization. Myo9b remains associated with dynamic F-actin for a considerable amount of time, although in vitro it spends a large fraction of its cycling time in the ATP-bound state (Nalavadi *et al.*, 2005; Kambara and Ikebe, 2006). The cycling time of Myo9b determined in vitro was ~0.5 s (Nalavadi *et al.*, 2005), and Myo9b was reported to move processively as a single-headed molecule (Inoue *et al.*, 2002; Post *et al.*, 2002; Nishikawa *et al.*, 2006). We did not observe directed movement of bleached or photoactivated Myo9b in the lamellipodium. This could be due to a relatively short run length of Myo9b. The in vitro velocity of actin gliding powered by Myo9b ranged from 20 to 80 nm/s at 25°C (Inoue *et al.*, 2002; Post *et al.*, 2002; O'Connell and Mooseker, 2003). This velocity is similar to the 25 nm/s retrograde actin flow observed in *Xenopus* cells viewed at 21–23°C (Watanabe and Mitchison, 2002). The similarities in velocity of actin flow and Myo9b movement could contribute to the difficulties in separating treadmilling of Myo9b holding on to actin and directed movement in the opposite (plus-end) direction. Alternatively, Myo9b may exist in two populations: one moving processively and the other one nonprocessively as documented by in vitro studies (Nalavadi *et al.*, 2005; Nishikawa *et al.*, 2006).

The finding that the Myo9b motor region positions the tail region with its RhoGAP activity to areas of actin polymerization implies that Myo9b will negatively regulate Rho signaling in these areas. Chemotactic migration of differentiated HL-60 cells, a neutrophil-like cell line, is dependent on low Rho activity and actin polymerization at the front and high Rho activity and acto-myosin contraction at the sides and back (Xu *et al.*, 2003; Wong *et al.*, 2006). Actin polymerization was found to be essential for suppressing RhoA activity. Because Myo9b is expressed abundantly in differentiated HL-60 cells (Wirth *et al.*, 1996), it is tempting to speculate that Myo9b could mediate the low RhoA activity at the front by associating with newly polymerizing F-actin providing a feedback mechanism for maintaining cell polarization. Depending on the directionality of Myo9b movement on actin filaments, it could either keep the RhoGAP domain close to the plasma membrane or aid in removing Rho from its site of action. A strikingly different spatiotemporal RhoA activation has been reported in randomly migrating fibroblasts in that RhoA activity was persistently high at the leading edge (Kurokawa and Matsuda, 2005; Pertz *et al.*, 2006). This might be explained not necessarily by the lack of a RhoGAP, but possibly by differences in available effector proteins or a faster cycling between active and inactive Rho due to differences in GEF protein activity. A

reciprocal balance between Rac and Rho activity has been described in fibroblasts and HEK cells (Sander *et al.*, 1999; Ohta *et al.*, 2006). Rac activity induces actin polymerization in the lamellipodium and antagonizes Rho activity. Myo9b could be part of a feedback mechanism by keeping Rho activity low in regions of actin polymerization, thus maintaining a balance between Rho and Rac activity supporting actin polymerization. The postulated role of Myo9b in sustaining actin polymerization can now be tested in further studies.

ACKNOWLEDGMENTS

We thank Pirta Hotulainen for cloning of pEGFP-Myo9b and initial live cell imaging experiments. The mRFP-actin plasmid was a generous gift of Roger Tsien (San Diego, CA) and Klemens Rottner (Braunschweig, Germany). Volker Gerke (Münster, Germany) and Klemens Rottner (Braunschweig) kindly gave us access to their TIRF microscopes. Margrit Müller, Ulrike Honnert, and Birgit Terstegge provided skillful technical assistance. The plasmid EGFP-Myo9b$^{ins-4A/GAP-}$ was constructed by Dinah Nockemann and Sandra Struchholz. Photoactivation experiments were performed at the Advanced Light Microscopy Facility (ALMF) of the European Molecular Biology Laboratory, Heidelberg, Germany. We thank the companies Olympus Europe (Hamburg, Germany) and Carl Zeiss (Göttingen, Germany) for continuous support of the ALMF. This work was supported by the Deutsche Forschungsgemeinschaft Grant SFB629/A2 to M.B.

REFERENCES

Ahmadian, M. R., Stege, P., Scheffzek, K., and Wittinghofer, A. (1997). Confirmation of the arginine-finger hypothesis for the GAP−stimulated GTP-hydrolysis reaction of Ras. Nat. Struct. Biol. *4*, 686–689.

Bähler, M. (2000). Are class III and class IX myosins motorized signalling molecules? Biochim. Biophys. Acta Mol. Cell Res. *1496*, 52–59.

Bejsovec, A. and Anderson, P. (1990). Functions of the myosin ATP and actin binding sites are required for *C. elegans* thick filament assembly. Cell *60*, 133–140.

Bernards, A. and Settleman, J. (2004). GAP control: regulating the regulators of small GTPases. Trends Cell Biol. *14*, 377–385.

Furch, M., Geeves, M. A., and Manstein, D. J. (1998). Modulation of actin affinity and actomyosin adenosine triphosphatase by charge changes in the myosin motor domain. Biochemistry *37*, 6317–6326.

Graf, B., Bähler, M., Hilpelä, P., Bowe, C., and Adam, T. (2000). Functional role for the class IX myosin myr5 in epithelial cell infection by *Shigella flexneri*. Cell. Microbiol. *2*, 601–616.

Grewal, P. K., Jones, A. M., Maconochie, M., Lemmers, R.J.F., Frants, R. R., and Hewitt, J. E. (1999). Cloning of the murine unconventional myosin gene Myo9b and identification of alternative splicing. Gene *240*, 389–398.

Inoue, A., Saito, J., Ikebe, R., and Ikebe, M. (2002). Myosin IXb is a single-headed minus-end-directed processive motor. Nat. Cell Biol. *4*, 302–306.

Joel, P. B., Trybus, K. M., and Sweeney, H. L. (2001). Two conserved lysines at the 50/20-kDa junction of myosin are necessary for triggering actin activation. J. Biol. Chem. *276*, 2998–3003.

Kambara, T. and Ikebe, M. (2006). A unique ATP hydrolysis mechanism of single-headed processive myosin, Myosin IX. J. Biol. Chem. *281*, 4949–4957.

Krementsova, E. B., Hodges, A. R., Lu, H., and Trybus, K. M. (2006). Processivity of chimeric class V myosins. J. Biol. Chem. *281*, 6079–6086.

Krendel, M. and Mooseker, M. S. (2005). Myosins: tails (and heads) of functional diversity. Physiology *20*, 239–251.

Kurokawa, K. and Matsuda, M. (2005). Localized RhoA activation as a requirement for the induction of membrane ruffling. Mol. Biol. Cell *16*, 4294–4303.

Moon, S. Y. and Zheng, Y. (2003). Rho GTPase-activating proteins in cell regulation. Trends Cell Biol. *13*, 13–22.

Müller, R. T., Honnert, U., Reinhard, J., and Bähler, M. (1997). The rat myosin myr 5 is a GTPase-activating protein for Rho in vivo: essential role of arginine 1695. Mol. Biol. Cell *8*, 2039–2053.

Murphy, C. T. and Spudich, J. A. (1999). The sequence of the myosin 50–20K loop affects Myosin's affinity for actin throughout the actin-myosin ATPase cycle and its maximum ATPase activity. Biochemistry *38*, 3785–3792.

Nalavadi, V., Nyitrai, M., Bertolini, C., Adamek, N., Geeves, M. A., and Bähler, M. (2005). Kinetic mechanism of Myosin IXB and the contributions of two class IX-specific regions. J. Biol. Chem. *280*, 38957–38968.

Nimnual, A. S., Taylor, L. J., and Bar-Sagi, D. (2003). Redox-dependent down-regulation of Rho by Rac. Nat. Cell Biol. *5*, 236–241.

Nishikawa, M., Nishikawa, S., Inoue, A., Iwane, A. H., Yanagida, T., and Ikebe, M. (2006). A unique mechanism for the processive movement of single-headed myosin-IX. Biochem. Biophys. Res. Commun. *343*, 1159–1164.

O'Connell, C. B., and Mooseker, M. S. (2003). Native Myosin-IXb is a plus-, not a minus-end-directed motor. Nat. Cell Biol. *5*, 171–172.

Ohta, Y., Hartwig, J. H., and Stossel, T. P. (2006). FilGAP, a Rho- and ROCK-regulated GAP for Rac binds filamin A to control actin remodelling. Nat. Cell Biol. *8*, 803–814.

Pertz, O., Hodgson, L., Klemke, R. L., and Hahn, K. M. (2006). Spatiotemporal dynamics of RhoA activity in migrating cells. Nature *440*, 1069–1072.

Post, P. L., Tyska, M. J., O'Connell, C. B., Johung, K., Hayward, A., and Mooseker, M. S. (2002). Myosin-IXb is a single-headed and processive motor. J. Biol. Chem. *277*, 11679–11683.

Potma, E. O., de Boeij, W. P., Bosgraaf, L., Roelofs, J., van Haastert, P. J., and Wiersma, D. A. (2001). Reduced protein diffusion rate by cytoskeleton in vegetative and polarized dictyostelium cells. Biophys. J. *81*, 2010–2019.

Reinhard, J., Scheel, A. A., Diekmann, D., Hall, A., Ruppert, C., and Bähler, M. (1995). A novel type of myosin implicated in signalling by rho family GTPases. EMBO J. *14*, 697–704.

Ridley, A. J. and Hall, A. (1992). The small GTP-binding protein rho regulates the assembly of focal adhesions and actin stress fibers in response to growth factors. Cell *70*, 389–399.

Sander, E. E., ten Klooster, J. P., van Delft, S., van der Kammen, R. A., and Collard, J. G. (1999). Rac downregulates Rho activity: reciprocal balance between both GTPases determines cellular morphology and migratory behavior. J. Cell Biol. *147*, 1009–1022.

Scheffzek, K., Ahmadian, M. R., and Wittinghofer, A. (1998). GTPase-activating proteins: helping hands to complement an active site. Trends Biochem. Sci. *23*, 257–262.

Shimada, T., Sasaki, N., Ohkura, R., and Sutoh, K. (1997). Alanine scanning mutagenesis of the switch I region in the ATPase site of *Dictyostelium discoideum* Myosin II. Biochemistry *36*, 14037–14043.

Tsuji, T. *et al.* (2002). ROCK and mDia1 antagonize in Rho-dependent Rac activation in Swiss 3T3 fibroblasts. J. Cell Biol. *157*, 819–830.

Tyska, M. J. and Mooseker, M. S. (2002). MYO1A (Brush Border Myosin I) dynamics in the brush border of LLC-PK1-CL4 cells. Biophys. J. *82*, 1869–1883.

Wang, H. R., Zhang, Y., Ozdamar, B., Ogunjimi, A. A., Alexandrova, E., Thomsen, G. H., and Wrana, J. L. (2003). Regulation of cell polarity and protrusion formation by targeting RhoA for degradation. Science *302*, 1775–1779.

Watanabe, N. and Mitchison, T. J. (2002). Single-molecule speckle analysis of actin filament turnover in lamellipodia. Science *295*, 1083–1086.

Weil, D., Levy, G., Sahly, I., Levi-Acobas, F., Blanchard, S., El-Amraoui, A., Crozet, F., Philippe, H., Abitbol, M., and Petit, C. (1995). Defective myosin VIIA gene responsible for Usher syndrome type IB. Nature *374*, 60–61.

Wirth, J. A., Jensen, K. A., Post, P. L., Bement, W. M., and Mooseker, M. S. (1996). Human myosin-IXb, an unconventional myosin with a chimerin-like rho/rac GTPase-activating protein domain in its tail. J. Cell Sci. *109*, 653–661.

Wong, K., Pertz, O., Hahn, K., and Bourne, H. (2006). Neutrophil polarization: Spatiotemporal dynamics of RhoA activity support a self-organizing mechanism. Proc. Natl. Acad. Sci. USA *103*, 3639–3644.

Xu, J., Wang, F., Van Keymeulen, A., Herzmark, P., Straight, A., Kelly, K., Takuwa, Y., Sugimoto, N., Mitchison, T., and Bourne, H. R. (2003). Divergent signals and cytoskeletal assemblies regulate self-organizing polarity in neutrophils. Cell *114*, 201–214.

Yengo, C. M. and Sweeney, H. L. (2004). Functional role of loop 2 in myosin V. Biochemistry. *43*, 2605–2612.